

Design Optimization Model for a
Schmidt-Cassegrain Telescope

ME 590 Final Report

Marc R. Zawislak

Optimal Design Laboratory

University of Michigan

Department of Mechanical Engineering

December 20, 2006

Chapter 1

Abstract

The goal of this project is to create a medium-sized multidisciplinary design optimization model that displays strong interactions in-between design variables. This model will be inputted into an automated coordination composition method that will show the tradeoffs of decomposing the problem in different arrangements.

A telescope product is used for the model. The telescope model chosen for this application is a consumer telescope consisting of two mirrors and a lens that an amateur astronomer could build.

The telescope model includes several different disciplines. First, the optics discipline is represented through a ray-tracing program which takes the system components and predicts the first-order and third-order optics. Next, a thermal subsystem represents the thermal displacement of several telescope parts as they are exposed to different thermal environments. Then, the performance of the system with manufacturing tolerances of several parts is examined with a cost model of the materials and manufacturing tolerances were developed to help show the 'price' for using more materials or tighter manufacturing tolerances. Finally, the tripod structure holding the telescope is modeled. The tripod is designed not to buckle, be tipped over easily, or easily clamp the telescope in position.

In conclusion the model has many different disciplines which should be able to be decomposed in different arrangements, thus showing the advantages of the optimal decomposition method.

Chapter 2

Nomenclature

Variable	Description	Units
t_{tube}	Thickness of the tube	m
D_{legs}	Diameter of the tripod legs	m
L_{legs}	Length of the tripod legs	m
D_{sch}	Diameter of Schmidt corrector and primary stop	m
D_1	Inner Diameter of tube and primary mirror	m
D_3	Diameter of secondary mirror	m
α_{tripod}	Tripod angle with ground	rad
Z_{sch}	Length of outside edge of schmidt corrector to primary mirror	m
ϵ_1	Eccentricity of primary mirror	
ϵ_2	Eccentricity of secondary mirror	
$Z_{mirrors}$	Location of secondary mirror	m
R_1	Radius of curvature of the vertex of primary mirror	m
R_2	Radius of curvature of the vertex of secondary mirror	m
v	Vertex of Back Focus	m
Z_{pivot}	Location of the pivot from primary mirror	m
h	Baffle optimization free parameter	m

$tol_{Z_{sch}}$	Tolerance of location of schmidt corrector	m
$tol_{Z_{mirrors}}$	Tolerance of location of secondary mirror	m
tol_{R_1}	Tolerance of radius of curvature of primary mirror	m
tol_{R_2}	Tolerance of radius of curvature of secondary mirror	m
tol_{ϵ_1}	Tolerance of eccentricity of primary mirror	m
tol_{ϵ_2}	Tolerance of eccentricity of secondary mirror	m
g	Acceleration of gravity	$\frac{m}{s^2}$
ρ_{tube}	Density of the tube	$\frac{kg}{m^3}$
t_{mirror}	Thickness of the mirror	m
ρ_{mirror}	Density of the mirrors	$\frac{kg}{m^3}$
ρ_{legs}	Density of the tripod legs	$\frac{kg}{m^3}$
ρ_{sch}	Density of the schmidt corrector	$\frac{kg}{m^3}$
CR_{tube}	Cost of material of outer tube	$\frac{\$}{m^3}$
CR_{sch_A}	A coefficient of cost of material of Schmidt corrector	
CR_{sch_B}	B coefficient of cost of material of Schmidt corrector	
CR_{mirror_A}	A coefficient(slope) of cost of material of mirrors	
CR_{mirror_B}	B coefficient(y-intercept) of cost of material of mirrors	
CR_{legs}	Cost of material of tripod legs	$\frac{\$}{m^3}$
$\alpha_{thermal_{tube}}$	Thermal coefficient of expansion of tube	$\frac{1}{\circ C}$
$\alpha_{thermal_{mirror}}$	Thermal coefficient of expansion of mirror	$\frac{1}{\circ C}$
ΔT	Temperature change	C
d_{plo}	Nominal thickness of the plate	m
numrays	Number of rays for ray-tracing	
E_{legs}	Young's Modulus of tripod leg material	Pa

CRA_{slot}	A cost coefficient of slotting manufacturing	
CRB_{slot}	B cost coefficient of slotting manufacturing	
CRA_{stamp}	A cost coefficient of stamping manufacturing	
CRB_{stamp}	B cost coefficient of stamping manufacturing	
Airy	Airy disk diameter	m
$time_{move}$	Time to move the telescope a specified distance	s
$F_{humanmax}$	Minimum force that can be exerted in moving the telescope	N
$max_{deadraysratio}$	Maximum ratio of dead rays/total rays	
F_{human}	Force human exerts on telescope during accident	N
$time_{human}$	Time the human exerts the force on telescope during accident	s
$MaxCost_{material}$	Maximum cost of materials	\$
$MaxCost_{tolerance}$	Maximum cost of the tolerancing	\$
$\frac{F}{\#}_{max}$	Maximum $\frac{Focal}{\#}$ range for Schmidt-Cassegrain	
$\frac{F}{\#}_{min}$	Minimum $\frac{Focal}{\#}$ range for Schmidt-Cassegrain	
τ_{max}	Maximum clamping torque that can be applied	$N - m$
$tol_{perform}$	Percentage of objective the tolerance limits must be within	
$Vert_{Llegs}$	Vertical height of tripod legs	m
q	Off-axis distance for spot diagrams	m
w	Angular Field of View	rad
\hat{m}_2	Integer in definition of characteristic function of SCT	
δS_I^*	Contribution of an aspheric plate to third order aberrations	

Chapter 3

Introduction to Telescopes

A telescope model was used to help demonstrate the objective of this project. This chapter gives an overview of the telescope system, their optics and examples of types of telescopes used by amateurs.

3.1 The Telescope System

A telescope product was initially chosen for the model. Telescopes can vary in size from a set of binoculars to the world's largest telescope in Mauna Kea, Hawai'i with mirrors 10 meters in diameter. Not only varying in size, telescopes can vary in complexity from a single lens to compound systems which are a combination of multiple mirrors and lenses. Telescope optics' origin dates back to the early seventeenth century being studied by professional optical designers. Until recently, amateur astronomers have not been involved in the telescope design process. However, with the development and availability of optical computer programs amateurs have been more interested in becoming involved in this process. Thus, this project will focus on a telescope that an amateur is capable of building.

An amateur telescope design can consist of designing many different parts. First, two types of optics devices can be included in telescopes: reflecting and refracting devices. Refracting devices change the velocity of the light while it is traveling through the medium. This causes the light rays to exit the medium at a different angle than entry. Since, different colored light travels at different wavelengths, the refractive angle varies with different colors. An example of a refracting device is a prism which disperses the rainbow as white light enters. A reflecting device is different from a refracting object as it does not allow the visible image to pass through it. Instead, it bounces back the image in the direction of its source at a different angle. An example of a reflecting device is a mirror.

A telescope system includes much more than just the lens and mirrors. First, a tube encloses its contents to protect the quality of the optical devices and holds them

in place. Next, telescopes include an eyepiece which enables the astronomer to be able to examine the image formed from the mirrors and lens. However, the eyepiece is so specialized that designing one in detail is another project in itself. Around each mirror, baffles are set up to help prevent stray light that is not desired by the astronomer to enter the eyepiece. These baffles can be compared to blinders that are put on a horse before a race to make sure they focus on the objective. Furthermore, a structure must hold the telescope in place to allow stationary viewing and stability. In most portable consumer telescopes, a tripod structure consisting of three legs secures the telescope in place. The tripod can prevent someone from easily knocking the telescope over or the wind causing vibrations while star gazing. Finally, there are many other smaller parts within a telescope that can be explained, however these are the main parts used in the telescope model. All of the main parts highlighted in this chapter will be discussed in more detail in our model analysis.

3.2 Telescope Optics

First order optics is a term concerning the optical analysis of rays with terms in the first order. This term describes how the light rays move within the desired mediums in a two-dimensional analysis. First order optics can be applied to a ray-tracing program to help examine the third order optics. Ray-tracing follows the rays algebraically as they are reflected or refracted throughout the telescope system. In this model the first order analysis is completed through a ray-tracing algorithm.

Third order optics is a term about image aberrations with optical terms in the third order. There are two types of aberrations: chromatic and monochromatic. Monochromatic aberrations are present in both refracting and reflecting systems and are not contingent of the wavelength. Monochromatic aberrations include: spherical aberration, coma, astigmatism, curvature of field, and distortion, which will explained in more detail in further sections. These aberrations can be measured analytically through a set of equations. Next, chromatic aberrations are present in refractive elements because the refractive index of glass is contingent on the wavelength. An example of this type of aberration can be witnessed in colors dispersing in a prism. Chromatic aberrations can be displayed through a series of plots called spot diagrams which is shown in figure 3.1. These spot diagrams will be used as our basis to determine the extent of the chromatic aberrations.

3.3 Types of Amateur Telescopes

Many different telescopes have been created throughout the four century long history. Two of the more popular reflective amateur telescopes and the most widely used

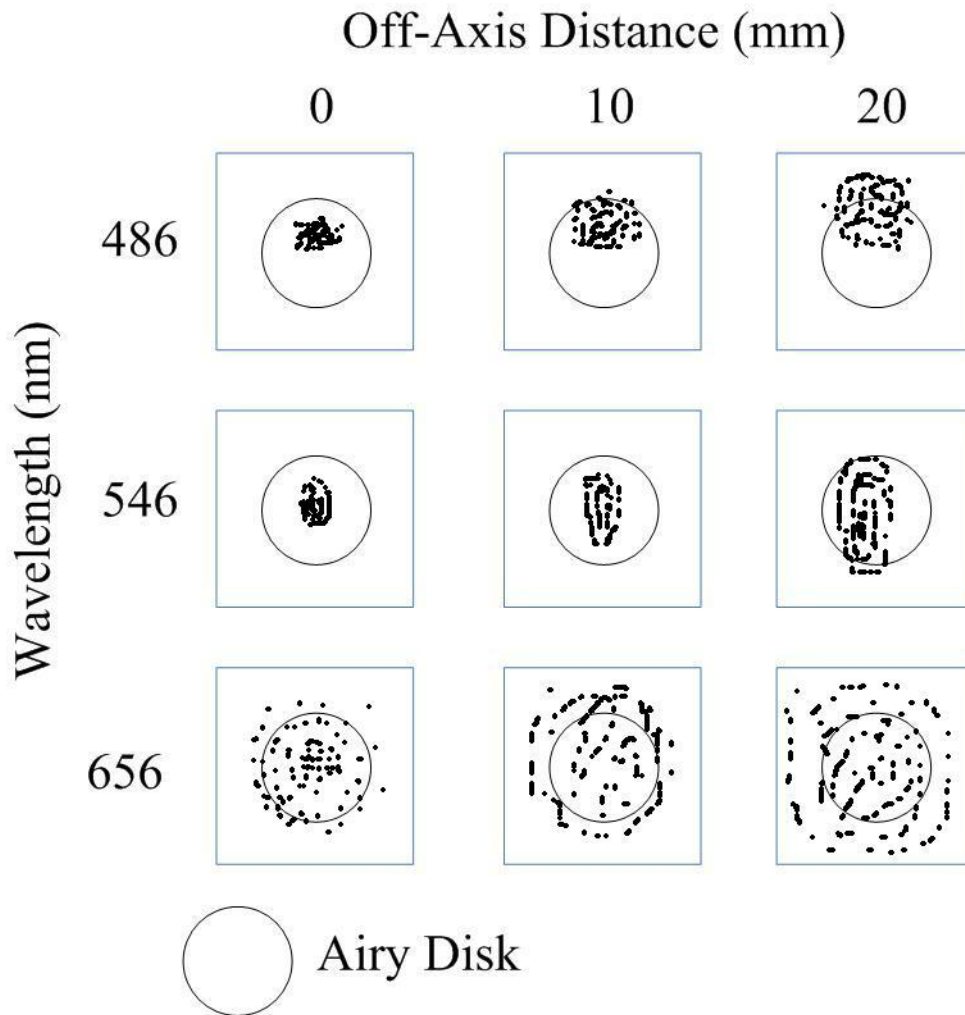


Figure 3.1: Example of a Spot Diagram

refractive lens will be discussed briefly in this section.

The Newtonian telescope is one of the simplest and most popular telescopes for amateur astronomers. The Newtonian telescope consists of two mirrors, a paraboloidal primary mirror and a flat secondary mirror as shown in figure 3.2. The focal surface where the astronomer views the image is above the tube. The secondary mirror centrally blocks light from traveling to the primary mirror. However, since the secondary mirror is at an angle it does not obstruct as much light as other telescopes. Unfortunately, by itself the telescope design suffers from monochromatic aberrations and other devices must be inserted to reduce these aberrations.

The Cassegrain telescope is another very popular telescope for amateur astronomers to build. The telescope is fairly similar to the Newtonian with two mirrors, however the focal surface is in back of the tube as compared with above for the Newtonian as shown in figure 3.3. In addition, both mirrors in a Cassegrain are spherical. Similar

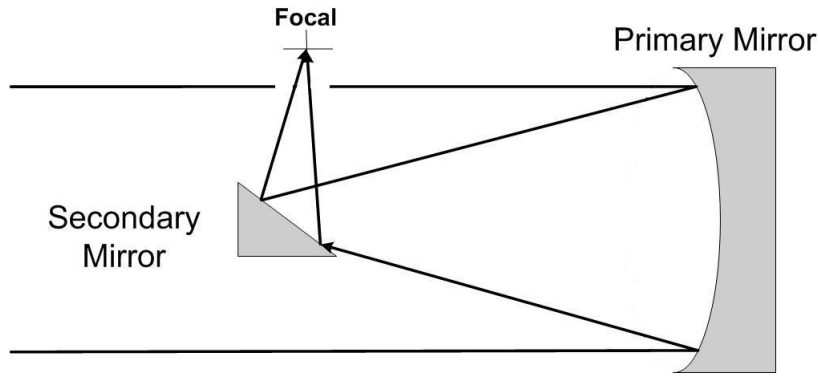


Figure 3.2: Optical Layout of Newtonian Telescope

to the Newtonian, the central obstruction causes a large loss of contrast and image sharpness. However, reducing the size of the secondary mirror can cause an increase in aberrations. Thus, the designer must review the tradeoffs of loss of light and the presence of aberrations in a Cassegrain system. Unwanted light can easily make its way into the focal area of a Cassegrain system, thus baffles must be introduced to block stray light. However, this further increases the loss of light entering the eye piece.

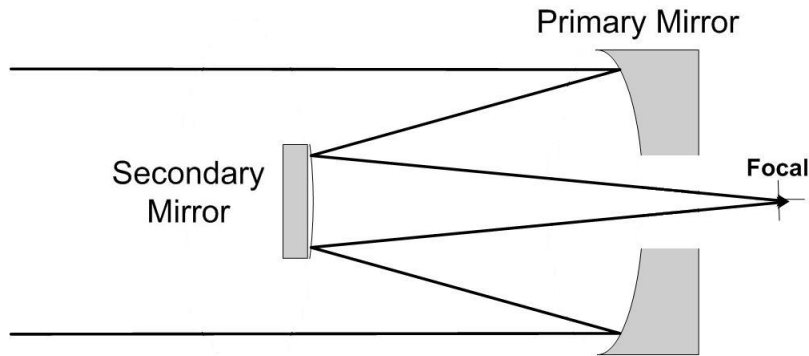


Figure 3.3: Optical Layout of Cassegrain Telescope

The Schmidt corrector is an aspheric refraction lens inserted to help reduce monochromatic aberrations with spherical mirrors. The profile of a Schmidt corrector dictates how the rays are refracted through the profile. However, since the corrector is a refracting element, it creates chromatic aberrations which can be measured through spot diagrams. The corrector lens is usually an addition to a telescope with a reflective surface.

The telescope type that will be modeled in this paper is a Schmidt-Cassegrain telescope(SCT). This is a very popular telescope among astronomers due to its compactness, transportability and excellent reduction of chromatic aberrations. The SCT combines the Cassegrain telescope with a Schmidt corrector for a total of three op-

tical components as shown in figure 3.4. The location of these components are free which gives a large design space for the designer. The SCT system consists of two strongly curved mirrors for our model. In addition, the Schmidt corrector helps reduce the amount of light loss with respect to the traditional Cassegrain telescope. This system will give us a very interesting optimization model as many different objects and disciplines rely on the same design variables of the system.

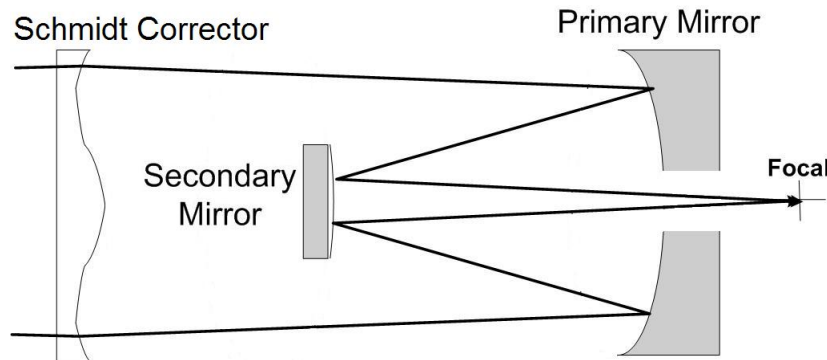


Figure 3.4: Optical Layout of Schmidt-Cassegrain Telescope without Baffles

The next chapter will explain the Schmidt-Cassegrain telescope model. It will give an overview of the telescope and the model for each of the discipline subsystems created for this model.

Chapter 4

Schmidt-Cassegrain Telescope

This chapter provides detail on the Schmidt-Cassegrain telescope algorithm and provides an overview of the analysis methods employed in this model.

4.1 Schmidt-Cassegrain Telescope System

The Schmidt-Cassegrain Telescope(SCT) is a very popular telescope to amateur astronomers. It consists of two mirrors and a refractive medium, a Schmidt corrector. Due to the number of parts, the design space or configurations of the telescope can vary. This will give a more interesting design problem as there is a large amount of space to examine.

Figure 4.1 is a picture of the Schmidt-Cassegrain telescope with our dimensioning of the design variables of the telescope. From this figure, all of the design variables that deal with the telescope and the baffle coordinates are shown in the z-y plane. It can be noted that zero of the z-axis begins at the location of the primary mirror and the zero of the y-axis is at the center line and the x-plane goes into the paper. Also, the centerline shows that the system is symmetrical. The dimensioned tripod can be found in figure 4.6. From the diagram, several geometric constraints can be determined. First, the length from the primary mirror to the Schmidt corrector must be greater than to the secondary mirror as shown in equation 4.1. Also, the inner diameter of the tube is defined to be the diameter of the primary mirror. Thus, the diameter of the aperture stop and Schmidt corrector must be less than that or it would be protruding through the tube as shown in equation 4.2.

$$Z_{sch} \leq Z_{mirrors} \quad (4.1)$$

$$D_1 \geq D_{sch} \quad (4.2)$$

The model comprises of several disciplines of the Cassegrain-Schmidt system.

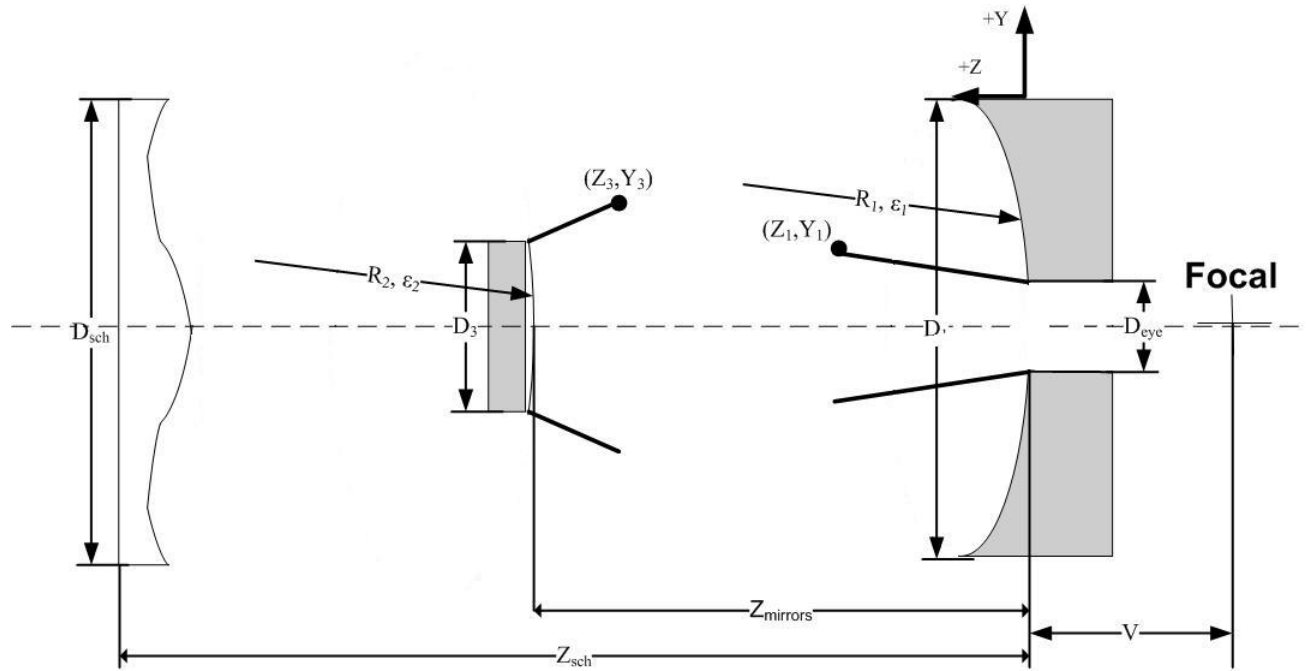


Figure 4.1: Dimensioned Drawing of Schmidt-Cassegrain Telescope

First, the optics discipline is represented through a ray-tracing program which takes into account the corrector lens and two mirrors and predicts the first-order and third-order optics. Next, a thermal subsystem represents the thermal displacement of several telescope parts as they are exposed to different thermal environments. Next, the performance of how the system reacts to the bounds of manufacturing tolerances of several parts is examined with a cost model of the materials and manufacturing tolerances to show the 'cost' for using more materials or tighter manufacturing tolerances. Finally, the tripod structure holding the telescope is modeled. The tripod is designed not to buckle, be tipped over easily, or easily clamp the telescope in position. All of these disciplines can be combined into one system to determine the true optimal design of the telescope.

4.1.1 Description of Objective Function

The objective function of system is to minimize the aberrations. The aberrations are viewed by the astronomer as a blurred image and can be caused by a variety of reasons. A visual method to view these aberrations are through a series of spot diagrams. An example of spot diagrams is shown in figure (reference) where each dot represents a single ray. The spot diagrams display what the image would look like at different off-axis distances and wavelengths. For visual use, the spread of the dots must be within a very small circle. The circle in which the light must encompass can be measured through an Airy disk which includes 84% of the energy in the image [6].

Thus, the Airy Disk will include the majority of the intensity of the image. The Airy disk is a function of the focal ratio of the system as shown in equation 4.3. Thus, the objective of the system is to minimize the amount of rays that are outside of the Airy disk for each of the spot diagrams. A penalty function for ray's distance away from the center was calculated to keep the objective continuous. Essentially, a ray within the Airy disk will be given a score of around zero and a ray outside the Airy disk will be given a penalty as shown in equation 4.4. This penalty has a very steep slope around the Airy disk boundary to simulate a discrete function as shown in figure 4.2 where the limit is 0.05 m.

$$Airy = 10^{-6}F_{\#} + 5 * 10^{-7} \quad (4.3)$$

$$\Phi(x, y, z, \lambda, q) = \frac{2000}{1 + e^{100000(\frac{Airy}{2} - spot(x,y,z,\lambda,q))}} \quad (4.4)$$

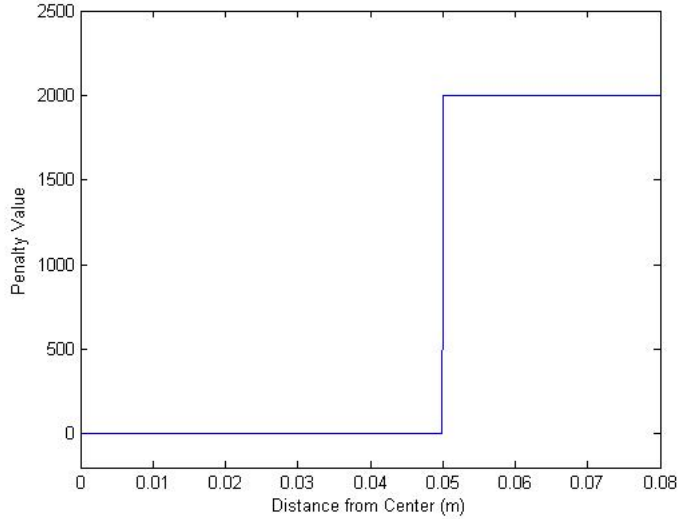


Figure 4.2: Graph of Airy Disk Penalty Function

The objective function is calculated from a total of nine spot diagrams and shown below. The three different wave lengths are shown in table 4.1 and the three different off-axis distances are zero, 10, and 20 mm.

$$\begin{aligned} \min_{\mathbf{x}} \quad & \sum_{q=1}^3 \sum_{\lambda=1}^3 \sum_{rays=1}^{numrays} \Phi(\mathbf{x}) \\ \text{subject to} \quad & g(\mathbf{x}) \leq 0 \\ & h(\mathbf{x}) = 0 \end{aligned}$$

Several equality and inequality constraints help limit the design bounds of the system. Most of the inequality constraints can be found throughout the model descriptions in equations 4.1, 4.2, 4.7, 4.8, 4.34, 4.44, 4.50, 4.51, 4.52, 4.53, 4.60, 4.62, 4.77, 4.80, 4.81, 4.83 and 4.87. The equality constraints can be found through the model descriptions in equations 4.18, 4.36, 4.37, 4.38, and 4.69.

An important system performance parameter considered with all telescopes is the focal ratio. The focal ratio is a ratio of the focal length of a mirror and the diameter of the aperture. It is a quantitative measure of the lens speed which is more important in photography settings. In telescope settings, the focal length controls the scale of the image that is presented at the eyepiece. Most telescopes are designed with a focal ratio specified, however for our model the focal ratio will be calculated from the radius of curvatures of the mirrors and the separation in-between mirrors. From [8], a range of suitable focal numbers is given for a Schmidt-Cassegrain telescope and acts as a constraint on a system as shown in equations 4.7 and 4.8.

$$\frac{1}{f'} = \frac{-f'_2 + f'_1 - Z_{mirrors}}{f'_1 f'_2} \quad (4.5)$$

$$\frac{F}{\#} = \frac{f'}{D_{sch}} \quad (4.6)$$

$$\frac{F}{\#_{max}} \geq \frac{F}{\#} \quad (4.7)$$

$$\frac{F}{\#_{min}} \leq \frac{F}{\#} \quad (4.8)$$

4.1.2 Ray-Tracing Algorithm

A ray-tracing algorithm is developed to determine what the image will look like for the astronomer through the eyepiece. Through the ray-tracing algorithm the objective function and spot diagrams can be developed. Furthermore, the spot diagrams can visually highlight any aberrations that are present in the system.

The first step in setting up the ray-tracing algorithm is giving an initial position for the rays. Figure 4.3 shows the location of all of the initial rays in a concentric pattern. The program will allow you to enter in the number of rays to be traced and it will develop the coordinates of each individual ray. Furthermore, all the coordinates must have three different wavelengths assigned to it. Furthermore, all the coordinates must have three different off-axis distances that will be used later in the ray-tracing program. In conclusion, for the coordinates of each ray there will be 3^2 different combinations that will be entered into the ray-tracing program as shown in our spot diagram figure 3.1 for the same $[x_0, y_0, z_0]$ coordinates.

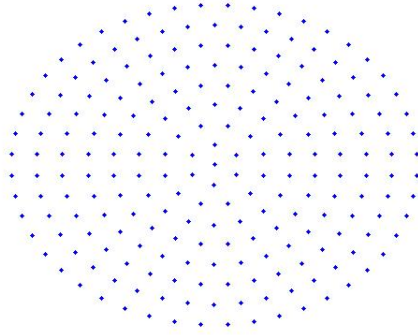


Figure 4.3: Concentric Initial Ray-Tracing Positions

The ray-tracing program is a multi-step process to determine the final ray location. First, the actual ray-tracing algorithm was gathered from Terebizh [7]. The actual equations will not be transcribed in this report, but they can be found in the referenced paper. However, several changes and additions must be made to this ray-tracing algorithm. First, the algorithm is for a cassegrain telescope and does not take into account the Schmidt corrector. Thus, the next section describes the addition for the Schmidt corrector. Next, Ray Tracing Algorithm Additions describes what additions to the ray-tracing algorithm was added on. Finally, Baffle Design and Algorithm describes how the baffle was designed and its impact on the ray-tracing algorithm.

Schmidt Corrector Ray Tracing

A Schmidt corrector was absent from the previously developed ray-tracing algorithm, thus it must be added in for our Schmidt-Cassegrain telescope. The Schmidt corrector will change the angle of the ray as it travels toward the primary mirror. Since the Schmidt corrector is a refractor, different wavelengths from the same entrance location will exit the corrector at different angles. As shown in figure 4.4, the profile of a Schmidt corrector is an aspheric surface. wavefront aberration in terms of radians can be expressed in for a corresponding refractive index n'_0 is shown in equation 4.9. n'_0 corresponds to a refractive index for wavelength λ_0 which is the benchmark, for our problem that will be the green wavelength. In addition, the new z-coordinate of our ray is going shown in equation 4.14 where 4.13 calculates the thickness of the Schmidt corrector.

$$(\delta W_I)_0 = \frac{1}{512} \frac{D_{sch}}{N^3} (\rho_{pl}^4 - k_{pl} \rho_{pl}^2) \quad (4.9)$$

where

$$N = \frac{-f'_1}{D_{sch}} \quad (4.10)$$

$$\rho_{pl} = \frac{y}{\frac{D_{sch}}{2}} \quad (4.11)$$

$$k_{pl} = \frac{y^2}{\left(\frac{D_{sch}}{2}\right)^2} \quad (4.12)$$

$$d_{pl} = \frac{1}{512} \left(\frac{1}{n'_0 - 1} \right) \frac{D_{sch}}{N^3} (\rho_{pl}^4 - k_{pl} \rho_{pl}^2) + (d_{pl})_0 \quad (4.13)$$

$$Z_1 = Z_{sch} - d_{pl} \quad (4.14)$$

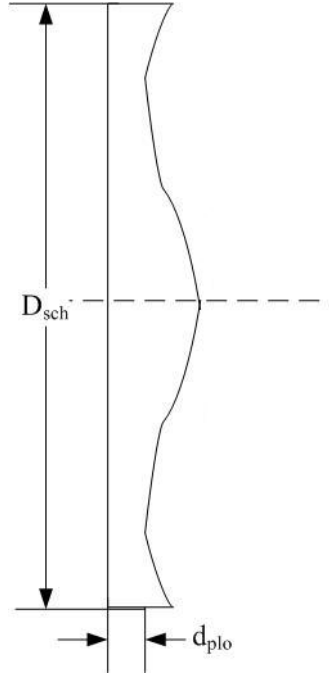


Figure 4.4: Profile of the Schmidt Corrector

Equation 4.15 determines the chromatic differential wavefront error for a given wavelength λ_1 and refractive index n'_1 . The three wavelengths and their refractive indexes in BK7 glass can be found in table 4.1. From the Schmidt corrector analysis, the angle and position of the ray entering the primary mirror can be calculated and added to the ray tracing algorithm.

$$(\delta W_I)_1 = \frac{n'_1 - 1}{n'_0 - 1} (\delta W_I)_0 \quad (4.15)$$

Ray-Tracing Algorithm Additions

As mentioned before the ray-tracing program is very similar to Terebizh's formulation. However, some differences for our example was adopted to make the formulation work. First, the original formulation is only is only in two dimensions, however our

Table 4.1: Color, Wavelengths, and Refractive Index of BK7 Glass

Color	Wavelength (nm)	Refractive Index
Red	656.27	1.51432
Green	546.07	1.51782
Blue	486.00	1.52238

ray-tracing program is in three dimensions. To solve this, it was assumed that the lens and mirrors would be symmetrical throughout the entire telescope tube. Thus, the initial y-coordinate in the algorithm can be computed by the distance from the x_1 and y_1 coordinate of the ray entering the system as shown in equation 4.16. Next, the algorithm gives a y-coordinate for the final ray through the eye-piece, however it does not give an x-coordinate. To solve for the x-coordinate, it is assumed the ray will converge toward the zero of the x-coordinate at the same rate as the y-direction. Thus, equation 4.17 expresses this with x and y as the initial ray coordinates and x_f and y_f as the final ray coordinates.

$$y_0 = \sqrt{x_1^2 + y_1^2} \quad (4.16)$$

$$x_f = \frac{y_f x}{y} \quad (4.17)$$

Baffle Design and Algorithm

A baffle system was designed in our system to help reduce stray light entering the telescope. The baffle system goal is to eliminate all the direct stray light entering the system without limiting the contrast and resolution of the object you are trying to view. Terebizh [7] has a optimal baffle algorithm which was used for this project. All the notation was taken directly that paper to reduce confusion. The only change is that the paper's x-coordinates are z-coordinates in this report. From Terebizh, the coordinates of the baffle design can be inputted into our system. Finally, one system equality constraint must be added to ensure the optimal baffle is designed as shown in equation 4.18.

$$\rho_{baf}(h) = [(Z_3 - Z_2)^2 + (Y_3 - Y_2)^2]^{\frac{1}{2}} = 0 \quad (4.18)$$

An algorithm must be developed to determine when the rays will intersect the baffle and not make it to the eyepiece. There are five different ways in which a ray may "die" and not make it into the eyepiece. In the programming, the ray must pass

all of the checkpoints to be deemed that it makes it to the eyepiece. A diagram of these scenarios can be found in figure 4.5

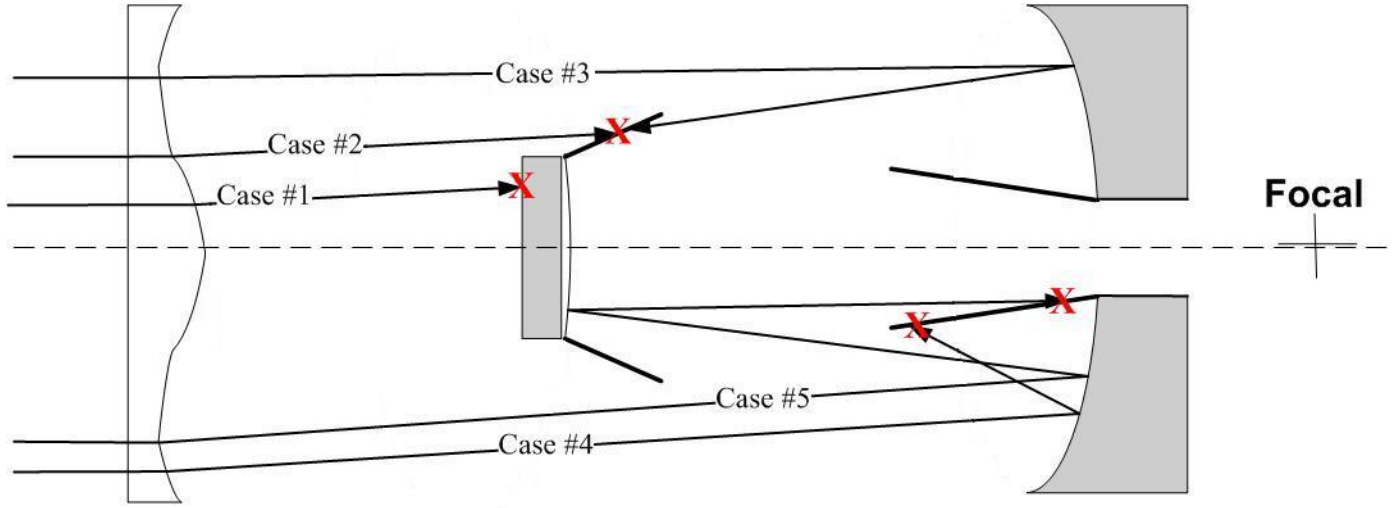


Figure 4.5: Scenarios of Rays Blocked by Baffles

Case #1 is if the ray hits the back of the secondary mirror. If the secondary mirror is too large it will prevent the rays from hitting the primary mirror and entering the eyepiece. To calculate this, we determined the y-position of the ray at $z=Z_{mirrors}$. If the position was less than half the diameter of the secondary mirror then the ray is eliminated. In conclusion if equation 4.19 is true, then the ray is eliminated.

$$b - \tan \alpha \leq \frac{D_3}{2} \quad (4.19)$$

Case #2 is that the ray hits the baffle attached to the secondary mirror before hitting the primary mirror. A line can be drawn from the secondary baffle corner to the secondary mirror with the slope of m_1 and y-intercept of b_1 . It is assumed the curvature in the secondary mirror in the z-direction is negligible. Thus, the algorithm determines when the line of the ray will intersect with the line of the secondary baffle at pos_2 . Then, if the position is in-between the start or end-position of the baffle then the intersection is real and the ray will be eliminated, if it is not in-between then the intersection will not occur. In conclusion, if equation 4.21 is true, then the ray is eliminated.

$$m_1 = \frac{(Y_3 - \frac{D_3}{2})}{(Z_3 - Z_{sch})} \quad (4.20)$$

$$b_1 = Z_3 - m_1 Y_3 \quad (4.21)$$

$$pos_2 = \frac{(b - b_1)}{(m_1 - \mu)} \quad (4.22)$$

$$Z_3 \geq pos_2 \geq Z_{mirrors} \quad (4.23)$$

Case #3 is that the ray hits the primary mirror, then hits the baffle attached to the secondary mirror before hitting the secondary mirror. Similar to the past two examples, a line is drawn from the secondary baffle corner to the secondary mirror with m_1 and b_1 . The equation of the line coming off the primary mirror is known. The algorithm determines when the line of the ray will intersect the line of the secondary mirror. If the intersection occurs within the coordinates of the baffle then the ray will be eliminated. Thus, if equation 4.25 is true, then the ray will be eliminated.

$$pos_3 = \frac{(a - b_1)}{(m_1 + k)} \quad (4.24)$$

$$Z_3 \geq pos_3 \geq Z_{mirrors} \quad (4.25)$$

Case #4 is that the ray hits the primary mirror, then hits the baffle attached to the primary mirror. This was calculated similarly to the past examples. However, now the ray must hit the primary baffle instead of the secondary baffle. The baffle attached to the primary mirror is described with a slope of m_2 and y-intercept of b_2 . Finally, if equation 4.29 is true, then the ray will be eliminated.

$$m_2 = \frac{(Y_1 - \frac{D_{eye}}{2})}{Z_1} \quad (4.26)$$

$$b_2 = \frac{D_{eye}}{2} \quad (4.27)$$

$$pos_4 = \frac{(a - b_2)}{(m_2 + k)} \quad (4.28)$$

$$Z_1 \geq pos_4 \geq 0 \quad (4.29)$$

Case #5 is that the ray hits the primary mirror and secondary mirror, then hits the baffle on the primary mirror. If equation 4.33 is true, then the ray will be eliminated.

$$m_3 = \frac{(Y_2 - \frac{l}{2})}{(s_2 - v)} \quad (4.30)$$

$$b_3 = y_2 - m_3 s_2 \quad (4.31)$$

$$pos_4 = \frac{(b_2 - b_3)}{(m_3 - m_2)} \quad (4.32)$$

$$Z_1 \geq pos_4 \geq -v \quad (4.33)$$

A count of all the rays that are eliminated is kept which is a performance criteria. Equation 4.34 calculates the ratio of rays that are eliminated with respect to the total number of rays. From [5], it is noted that the number of rays that are eliminated should be no more than 30% as represented by the parameter *maxdeadraysratio*.

$$\frac{deadrays}{rays_{total}} \leq max_{deadraysratio} \quad (4.34)$$

4.2 Third-Order Aberrations

Aberrations within the system lead to reduced optical quality. An ideal optical system would produce a point image for the astronomer's eyes if the source was a star. However, in most cases a blurred circle is obtained where it is a combination of different kinds of aberrations. As explained earlier, there are two types of aberrations: chromatic and monochromatic. Chromatic aberrations are a function of the color of light or wavelength of the light entering in the system. While monochromatic aberrations will be the same for all types of wavelengths entering in the system. The following sections will discuss chromatic and monochromatic aberrations and how they are calculated for our model.

4.2.1 Chromatic Aberrations

Chromatic aberrations occur in refracting light as a function of the specific wavelength. Chromatic aberrations cannot be solved analytically like monochromatic aberrations. Thus, they can be viewed as spot-diagrams with varying wavelengths and off-axis angles. The spot-diagram is the objective function and can be described in section 4.1.1.

4.2.2 Monochromatic Aberrations

Monochromatic aberrations occur in both refracting and reflecting with respect to one wavelength. The Seidel aberrations were developed in the 1850's where ΣS_I deals with spherical aberration, ΣS_{II} is coma, and ΣS_{III} is astigmatism from [8]. For all of the necessary aberrations to be eliminated they must all be equal to zero as shown in equation 4.35. Equations 4.36, 4.37 and 4.38 are equality constraints that will eliminate all of the monochromatic aberrations. The spherical aberration, coma and astigmatism are represented by equations 4.36, 4.37 and 4.38 respectively. Finally, equation 4.44 limits the necessary asphericity for the aspheric plate with relation to the focal length of the primary mirror and is a system inequality.

$$\Sigma S_I = \Sigma S_{II} = \Sigma S_{III} = 0 \quad (4.35)$$

$$-f'\zeta + L\xi + \delta S_I^* = 0 \quad (4.36)$$

$$-d_1\xi - \frac{-f'}{2} + \frac{s_{pl}}{f'}\delta S_I^* = 0 \quad (4.37)$$

$$\frac{f'}{L}(f' + d_1) + \frac{d_1^2}{L}\xi + \left(\frac{s_{pl}}{f'}\right)^2\delta S_I^* = 0 \quad (4.38)$$

where

$$\xi = \frac{(\hat{m}_2 + 1)^3}{4} \left(\frac{\hat{m}_2 - 1}{\hat{m}_2 + 1} \right)^2 \quad (4.39)$$

$$\zeta = \frac{\hat{m}_2^2}{4(1 - \epsilon_1^2)} \quad (4.40)$$

$$d_1 = Z_{mirrors} \quad (4.41)$$

$$L = v - Z_{mirrors} \quad (4.42)$$

$$s_{pl} = -Z_s ch f' \quad (4.43)$$

$$\delta S_I^* \leq \frac{-f'_1}{4} \quad (4.44)$$

It must be noted that it might be very difficult to satisfy all three of the equality constraints. Baker [8] proposed that only four different SCT configurations can be devised to eliminate all three aberrations which would greatly reduce the design space. Thus, it might suggested to relax these equality constraints to inequality constraints with some slack to create a more interesting design problem.

4.3 Thermal Displacement

The telescope can be used in different temperature environments which will effect the performance. Thermal expansion or compression will result in misalignments of the parts and aberrations within the system. The system is designed for room temperature, however the telescope could be brought outside during a cold night or used in very hot conditions. Thus, both cases must be investigated. Thermal displacements were taken into account for the outside tube. This effected the positioning of the Schmidt corrector and secondary mirror. The displacements were added to the manufacturing tolerances explained in section 4.4.

4.3.1 Thermal Displacement of Tube

The outside tube of the telescope will displace with changes to the temperature. This will cause the components inside the tube to change their positions which will in effect cause aberrations. In this section, we will measure how far the components will change positions as a function of temperature change. The effect of the changes on the performance will be calculated in the manufacturing tolerances in section 4.4. Equation 4.45 calculates the thermal elongation of the entire tube due to a change in temperature ΔT of $20^\circ C$. Equation 4.46 and 4.47 calculate the thermal displacement for position of the Schmidt corrector and secondary mirror. It was assumed the tube would be made out of Wrought Aluminum Alloy 7050, T7451 with a thermal expansion ($\alpha_{thermal_{tube}}$) of $23.6 \cdot 10^{-6} \frac{1}{^\circ C}$ ([1]). Finally, Since the primary mirror is at reference axis it is assumed it will stay at that position.

$$\delta_{tube} = \alpha_{thermal_{tube}} \Delta T Z_{tube} \quad (4.45)$$

$$\delta_{sch} = \frac{\delta_{tube} Z_{Sch}}{Z_{tube}} \quad (4.46)$$

$$\delta_{mirrors} = \frac{\delta_{tube} Z_{mirrors}}{Z_{tube}} \quad (4.47)$$

4.4 Manufacturing Tolerances and Cost Modeling

The manufacturing tolerances of the components in the system were taken into consideration. A system without tolerances is very unrealistic as the parts cannot be manufactured and assembled to the exact dimensions they are specified. However to show the tradeoffs of tighter tolerances, a cost model must be developed simulating the cost of increased tolerances. Thus, this section will explain the computation of the manufacturing tolerances and their respective cost model.

4.4.1 Tolerances of Mirror

This section summarized how the performance is measured for the tolerances due to thermal displacement and manufacturing processes. First, the tolerances are considered for six design variables:

- (1) Eccentricity of the primary mirror (ϵ_1)
- (2) Eccentricity of the secondary mirror (ϵ_2)
- (3) Radius of curvature of the vertex of primary mirror (R_1)
- (4) Radius of curvature of the vertex of secondary mirror (R_2)
- (5) Location of the secondary mirror ($Z_{mirrors}$)

(6) Location of the Schmidt corrector (Z_{sch})

The manufacturing processes to create each of these parts and design variables were considered. It is assumed the Schmidt corrector and secondary mirror will be placed by a slotting action in the tube. Thus, from CES [1] the tolerances that can be obtained for slotting is 0.00002 to 0.005 m . A stamping process will be cutting out the material forming the secondary and primary mirrors. Thus, the available tolerances that can be obtained for stamping is from 0.0001 to 0.0008 m [1]. Next, the tolerances must be added when applied to the design variables and the telescope's performance must be analyzed. In addition, the tolerances can include the thermal displacement that were calculated in section 4.3.1. As a function of the temperature change the material could expand or contract, thus the thermal displacement of the material is summed in the total tolerance

The performance of the telescope was analyzed for two different tolerance scenarios: the maximum positive and negative cases. The maximum positive case is when all the design variables are at the tolerance bounds in the positive direction. The negative case is in the same line of thought except the tolerances are subtracted. For example, a part that is 1 ± 0.05 . For the positive case, the part's dimension would be 1.05 while for the negative case the part's dimension would be 0.95. Since, some of the design variables are already negative, the positive case would increase the length of the object, for example from -1 to -1.05. For the thermal displacement, the positive case would be for thermal expansion while the negative case is for contraction. This can be shown in equation 4.48 for the positive tolerances and 4.49 for the negative tolerances. It was concluded that this method would be able to examine the two extremes of the design space from the nominal value to both bounds of the tolerances. Possibly, a Monte Carlo simulation of the design space can determine if there are any tolerance combinations that reduce the performance more.

$$\epsilon_{1_{hbound}} = \epsilon_1 + tol_{\epsilon_1} + \delta_{\epsilon_1} \quad (4.48)$$

$$\epsilon_{1_{lbound}} = \epsilon_1 - tol_{\epsilon_1} - \delta_{\epsilon_1} \quad (4.49)$$

The dimensions of the new toleranced design variable values and other design variables are entered into the ray-tracing algorithm. So, the ray-tracing program is called three times in total, once with the nominal values and twice with the tolerance dimensions. From the ray-tracing program, a new penalty function value will be calculated for both tolerance scenarios which will be compared with the penalty value of the nominal system. The positive and negative tolerance penalty values must be within a certain percent of the nominal objective function as shown in the constraints 4.50 and 4.51. In addition, the number of rays that are eliminated by the baffles must be within the same range to ensure the sharpness as shown in equation 4.52

and 4.53. These inequalities ensure that the tolerated model's performance criteria is within a certain percent nominal values.

$$obj_{hbound} \leq tol_{perform} obj_{nominal} \quad (4.50)$$

$$obj_{lbound} \leq tol_{perform} obj_{nominal} \quad (4.51)$$

$$\frac{deadrays_{hbound}}{rays_{total}} \leq tol_{perform} max_{deadraysratio} \quad (4.52)$$

$$\frac{deadrays_{lbound}}{rays_{total}} \leq tol_{perform} max_{deadraysratio} \quad (4.53)$$

4.4.2 Cost Modeling of Manufacturing Tolerances

A cost model of the manufacturing tolerances was developed to help show the trade-offs of tighter tolerances. In addition, this formulation will help prioritize which dimensions will be allocated more money for tighter tolerances based on the optical performance. It has been noted [2] that cost modeling for manufacturing tolerances can be calculated in many different formulations. The general cost formulation of the manufacturing tolerances for this model is a reciprocal function and shown in equation 4.54 where A and B are constants and T is the manufacturing tolerance of the dimension. Since, the manufacturing tolerances cost is site specific, a baseline cost was set up for one of the manufacturing processes and the other process was priced with respect to baseline.

$$C_m = A + \frac{B}{T} \quad (4.54)$$

The cost of the manufacturing tolerances for the placement of the Schmidt corrector and secondary mirror were calculated similarly. In addition, this manufacturing process was used as the baseline for the other process to be compared with. The manufacturing cost of slotting is calculated in equation 4.55 where CRA_{slot} is equal to 1 and CRB_{slot} is equal to 0.005. For the tolerance ranges of slotting, the cost of producing the tolerances is from \$11 to \$211 for each action. However, the tolerances can be different for each of the two cutting components, thus total cost for slotting is calculated within 4.59 where the costs are a function of the tolerance of the position of the Schmidt corrector and secondary mirror.

$$C_{slot} = CRA_{slot} + \frac{CRB_{slot}}{T_{slot}} \quad (4.55)$$

$$C_{tot_{slot}} = C_{slot}(T_{Z_{sch}}) + C_{slot}(T_{Z_{mirrors}}) \quad (4.56)$$

The cost of manufacturing the eccentricity and curvature of radiuses of the primary and secondary mirror were calculated similarly. It was decided the stamping process would be more expensive than the slotting process for both the initial cost and producing tighter tolerances. The manufacturing cost was calculated in equation 4.57 where CRA_{stamp} is equal to 10 and CRB_{stamp} is equal to 0.05. For the range of tolerances for stamping, the cost of the tolerances range is \$72.50 to \$510. The tolerances can be different for all four of the stamping components, thus the total cost for cutting is calculated within equation 4.59.

$$C_{stamp} = CRA_{stamp} + \frac{CRB_{stamp}}{T_{stamp}} \quad (4.57)$$

$$C_{totstamp} = C_{stamp}(T_{\epsilon_1}) + C_{stamp}(T_{\epsilon_2}) + C_{stamp}(T_{R_1}) + C_{stamp}(T_{R_2}) \quad (4.58)$$

The total cost for allocating tolerances can be seen in equation 4.59. This takes into account six different design variables that tolerances are allocated to. Finally, the constraint in equation 4.60 limits how much money can be spent on precise tolerances.

$$cost_{tolerance} = C_{totslot} + C_{totstamp} \quad (4.59)$$

$$MaxCost_{tolerance} \geq cost_{tolerance} \quad (4.60)$$

4.5 Material Cost Modeling

A cost model of the materials used to build the telescope system was developed to show the tradeoffs a consumer or company might go through in their decision making model. The cost model takes into account the following parts of the telescope:

- (1) Outer Tube
- (2) Schmidt Corrector
- (3) Primary and Secondary Mirrors
- (4) Tripod Legs

The cost of these prices are assumed to be at bulk rate and gathered from a variety of sources ([1], [3], [4]). The total cost of the system can be seen in equation 4.61. A system constraint limiting the amount of money that can be spent on materials was placed to illustrate the tradeoffs that would be placed on the system constraint. The constraint can be found in equation 4.62 where $MaxCost_{material}$ is the maximum amount of money that can be spent on materials.

$$Cost_{material} = C_{tube} + C_{sch} + C_{mirrorp} + C_{mirrors} + C_{legs} \quad (4.61)$$

$$MaxCost_{material} \leq Cost_{material} \quad (4.62)$$

4.5.1 Cost of Telescope Tube

Cost of the telescope tube is calculated to show the tradeoffs of using a shorter telescope. The tube is assumed to be made from a sheet of metal, then the metal is formed around a cylinder so that no material is cut out of the middle and lost during the process. Also, the tube is made from Wrought Aluminum Alloy 7050, T7451. The material and cost properties are taken from CES [1] with the density being 2823 ($\frac{kg}{m^3}$) and a price of 1.926 ($\frac{\$}{kg}$). These two values are multiplied together to determine the cost of material price per volume for the outer tube (CR_{tube}). Furthermore, the cost of material for the tube can be found in equation 4.63.

$$C_{tube} = CR_{tube}(-Z_{tube}) \frac{\pi((D_{tube} + t_{tube})^2 - D_{tube}^2)}{4} \quad (4.63)$$

4.5.2 Cost of Tripod Legs

The description of the cost of the tripod legs is described in this section. First, it is assumed the tripod legs are solid cylindrical shaped tubes and all three legs are similar. Next, the legs are made from carbon fiber reinforced carbon matrix composite (Vf: 50%) where the material and cost properties are taken out of the CES Database [1] with the density being 1700 ($\frac{kg}{m^3}$) and a price per mass of 217 ($\frac{\$}{kg}$). If the cost of these legs become to large it would be suggested to change to a more economical material. These two values are multiplied together to determine the cost per volume of material for the legs (CR_{legs}). Finally, the cost of material for all three tubes can be found in equation 4.64.

$$C_{legs} = 3CR_{legs}L_{legs} \frac{\pi D_{legs}^2}{4} \quad (4.64)$$

4.5.3 Cost of Primary and Secondary Mirrors

The cost of the primary and secondary mirror is calculated to show tradeoffs of larger sized mirrors. In addition, this will show the tradeoffs in-between smaller and cheaper mirrors and optical performance. Since, a large amount of post-processing is involved in building a mirror, the material costs are approximated from retail prices of current mirrors. It is assumed the mirrors are made out of the material Pyrex[®]. In addition, it is assumed the materials for the primary and secondary mirrors will be the same with the only difference being a hole will be drilled through the primary mirror for the eyepiece. However, this drilling cost is not taken into account. Next,

prices for spherical mirrors with varying diameters were taken [3] and their data can be found in table 4.2. From graphing this data, a linear line was chosen to model the trendline, where two coefficients would be the slope and y-intercept, CR_{mirror_A} and CR_{mirror_B} respectively. Finally, the cost of the primary and secondary mirror is shown in equation 4.65 and 4.66 where $CR_{mirror_A} = 366.1$ and $CR_{mirror_B} = -20.1$.

Table 4.2: Diameter and Price of Spherical Mirrors

Diameter(m)	Price
0.102	\$17.50
0.152	\$36.75
0.203	\$51.00
0.254	\$74.75

$$C_{mirrorp} = CR_{mirror_A}D_1 + CR_{mirror_B} \quad (4.65)$$

$$C_{mirrorp} = CR_{mirror_A}D_3 + CR_{mirror_B} \quad (4.66)$$

4.5.4 Cost of Schmidt Corrector

The cost of the Schmidt corrector is very important as this is a very expensive piece in a Schmidt-Cassegrain telescope. It has been noted the price of Schmidt correctors increase exponentially with larger diameters due to the precise cutting of the glass that must be completed to the aspheric plate [4]. It is assumed that the plate is made out of PK3 glass as this is one of the cheaper industry preferred materials for refractive lenses. Next, the prices and diameters of the aspheric plates were recorded and plotted as shown in table 4.3. It was assumed the retail prices can be divided by four to take into account the price mark-up. From the plot of price vs. diameter an exponential line best fits with the data. Two coefficients are developed to plot these lines: CR_{sch_A} and CR_{sch_B} with values of 3.4727 and 23.415 respectively. Finally, the cost of the Schmidt corrector is shown in 4.67 as a function of the diameter of the Schmidt corrector.

$$C_{mirrorp} = CR_{sch_A}e^{CR_{sch_B}D_{sch}} \quad (4.67)$$

Table 4.3: Diameter and Price of Spherical Mirrors

Diameter(m)	Price
0.018	\$5.75
0.024	\$6.25
0.034	\$6.50
0.05	\$11.25
0.06	\$15

4.6 Tripod Structural Analysis

An important subsystem of this model is the tripod structural system. The tripod system assists in solving for several variables within the tripod system, while taking into account the telescope subsystem. This helps to create coupling in-between the tripod and telescope design variables. The tripod structure design takes into account:

- (1) Designing the telescope to be a certain height
- (2) Design against the legs buckling
- (3) Design against being tipped over
- (4) Design for reduced clamping force
- (5) Design for minimal moving force

Tradeoffs are introduced by attempting to reduce material costs while keeping a structurally sound system. In addition, a couple analyses will drive the telescope to weigh less. A picture of our tripod design can be seen in figure 4.6. Each section will describe how each of these requests were accomplished.

4.6.1 Design Telescope for Height

The tripod legs dictate at what height the telescope will be viewed at by the astronomer. A telescope that is low can cause discomfort to a user when they bend down too much. Also, a telescope that is too high will not be able to be used by younger astronomers. Thus, it was determined that the vertical telescope height($Vert_{L_{Legs}}$) will be 1.3 meters. From equation 4.68, the length of the tripod leg can be determined. Equation 4.69 will be an inequality constraint in our system.

$$L_{legs} = \frac{Vert_{L_{legs}}}{\sin(\alpha_{tripod})} \quad (4.68)$$

$$L_{legs} = Vert_{L_{Legs}} \quad (4.69)$$

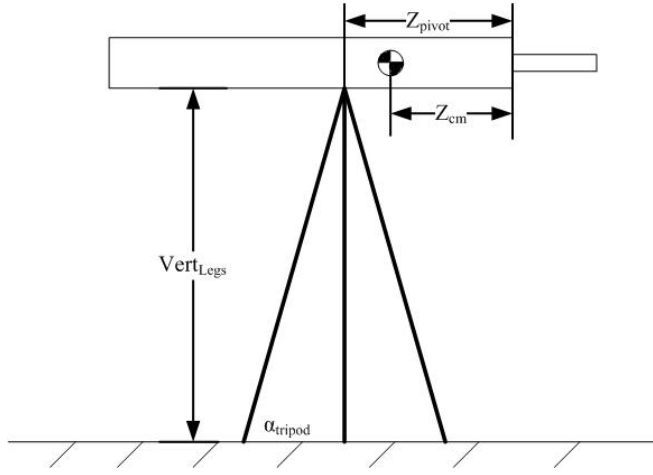


Figure 4.6: Schematic Drawing of Tripod Dimensions

4.6.2 Design Tripod Legs against Buckling

The tripod legs must be designed so they do not buckle under the mass of the telescope. To accomplish this, the gravitational force of mass of the telescope components must be calculated as shown in equations 4.70 through 4.74. It is assumed the force will be spread equally throughout all three legs of the tripod and since the tripod lays at an angle, the resultant force in each tripod leg is calculated in equation 4.75. Finally, the buckling force of a leg as a function of its dimensions and Young's Modulus is found in equation 4.76 where $n = 1$ for a pinned cantilever beam. The constraint is equation 4.77, limits the force that can be put in the through each leg assuming a 1.5 safety factor.

$$F_{tube} = g\rho_{tube}Z_{tube} \frac{\pi((D_{tube} + t_{tube})^2 - D_{tube}^2)}{4} \quad (4.70)$$

$$F_{sch} = g\rho_{sch}d_{plo} \frac{\pi(D_{sch})^2}{4} \quad (4.71)$$

$$F_{mirrors} = g\rho_{mirror}t_{mirror} \frac{\pi(D_3)^2}{4} \quad (4.72)$$

$$F_{mirrorp} = g\rho_{mirror}t_{mirror} \frac{\pi(D_1)^2}{4} \quad (4.73)$$

$$F_p = F_{tube} + F_{sch} + F_{mirrorp} + F_{mirrors} \quad (4.74)$$

$$F_{leg} = \sqrt{\frac{F_p^2}{3} (1 + 2(\sin(\alpha_{tripod}))^2)} \quad (4.75)$$

$$Buck_{force} = \frac{n^2\pi^3 ED_{leg}^4}{64L_{leg}^2} \quad (4.76)$$

$$Buck_{force} \geq 1.5F_{leg} \quad (4.77)$$

4.6.3 Design Tripod Legs against Tipping Over

The tripod must be designed against tipping over very easily if someone knocks into it. To prevent the telescope from tipping over, the center of mass of the telescope must never be on the outside of the tripod leg in contact with the ground. If the center of mass is outside, gravity will cause the telescope to tip over. First, the center of mass of the telescope must be calculated using the masses and locations of all of the components as shown in equation 4.78. Next, it is assumed a human bumps into the telescope for a time of $time_{human}$ seconds applying a force of F_{human} . The distance traveled by the telescope is a kinematic relation as shown in equation 4.79. Finally, a constraint states the distance traveled by the telescope must be less than the distance from the location of the pivot to the end of the tripod as shown in equation 4.80 and 4.81.

$$Z_{cm} = \frac{F_{tube}(-\frac{Z_{tube}}{2}) + F_{sch}Z_{sch} + F_{mirrors}Z_{mirrors}}{F_p} \quad (4.78)$$

$$dist = \frac{F_{human}}{m_{tele}}time_{human}^2 \quad (4.79)$$

$$Z_{pivot} - \cos(\alpha_{tripod})L_{legs} \geq Z_{cm} - dist \quad (4.80)$$

$$Z_{pivot} + \cos(\alpha_{tripod})L_{legs} \leq Z_{cm} + dist \quad (4.81)$$

4.6.4 Design for Reduced Clamping Torque

The telescope must be designed so the stars can be easily viewed by the astronomers. One aspect of accomplishing this is to allow the telescope to be easily clamped in position for the astronomer to attempting to view a star. Thus, the force needed to clamp the telescope must be small enough a human will be able to tighten it by their hands. The clamping force is a function of the mass of the telescope and the distance in-between the center of mass and the pivot. Due to the direction of gravity, the maximum clamping force would be necessary when the telescope is parallel with the ground. It assumed the clamping torque must be equal to the resistance torque which is the distance in-between the center of mass and the pivot support as shown

in equation 4.82. A parameter was assigned to the maximum clamping torque that can be applied by a human, τ_{max} . Finally, a constraint is put into place saying the maximum clamping torque by a human must be greater than the resistance torque in both directions in equation 4.83.

$$Resist_{\tau} = (Z_{pivot} - Z_{cm})m_{tele} \quad (4.82)$$

$$\tau_{max} \geq Resist_{\tau} \geq -\tau_{max} \quad (4.83)$$

4.6.5 Design for Minimal Moving Force

The telescope must be designed to reduce the amount of force necessary to move it. To accomplish this a position pattern in a specified amount of time was required to move the telescope. The position pattern was moving the telescope 180 deg in the x-plane and 45 deg in the z and y-plane. Assuming the telescope would be gripped at the end of the telescope to get the maximum amount of torque, the total distance the telescope must be moved is in equation 4.84. Next, it is assumed the user will not want to be spending a long time moving the telescope this distance, thus a time ($time_{move}$) to move the telescope is specified. From kinematic properties the constant acceleration can be measured in equation 4.85. Next, the force necessary to move the telescope with that acceleration is shown in equation 4.86. Finally, this force necessary must be less than what a human can exert as shown in 4.87.

$$d_{move} = -Z_{pivot}\pi\sqrt{\frac{3}{8}} \quad (4.84)$$

$$a_{move} = \frac{2d_{move}}{t_{move}^2} \quad (4.85)$$

$$F_{nec} = \frac{m_{tele}a_{move}(Z_{pivot} - Z_{cm})}{Z_{pivot}} \quad (4.86)$$

$$F_{humanmax} \geq F_{nec} \quad (4.87)$$

Chapter 5

Comments

The comments section gives an overview of the system to be used as optimization practice. This section will give a table of the design variables with suggested lower and upper bounds. Next, the performance parameters will be listed with suggested values for them. Finally, hard parameters will be listed their their values which should not change.

5.1 Design Variables

The design variables are listed in table 5.1. In total, there are 23 design variables with the lower and upper bounds shown below. If the optimal design is hitting the bounds and the result makes sense you can change the bounds so you will get an interior optimum.

5.2 Performance Parameters

The performance parameters and their suggested values are listed in table 5.2. Performance parameters are defined as parameters which define the performance of the telescope. Thus, these suggested values can be changes if you would like to make the telescope more competitive against the market.

5.3 Hard Parameters

The hard parameters of the system and their suggested values can be found in table 5.3. Hard parameters are defined as parameters in which either represent a material property or other value that it is not recommended to change. However, with the proper research these values may be change to sculpt the design space.

Table 5.1: Design Variables with Lower and Upper Bounds

Variable	Lower Bound	Upper Bound	Units
D_{legs}	0.000001	0.1	m
L_{legs}	1.3	5	m
D_{sch}	0.01	1	m
D_1	0.01	1	m
D_3	0.01	1	m
α_{tripod}	0	$\frac{\pi}{2}$	rad
Z_{sch}	-4	-0.01	m
ϵ_1	-3	3	
ϵ_2	-3	3	
$Z_{mirrors}$	-4	-0.01	m
R_1	-20	0	m
R_2	-20	0	m
v	0	2	m
Z_{pivot}	-4	0	m
h	0	4	m
$tol_{Z_{sch}}$	0.00002	0.005	m
$tol_{Z_{mirrors}}$	0.00002	0.005	m
tol_{R_1}	0.0001	0.0008	m
tol_{R_2}	0.0001	0.0008	m
tol_{ϵ_1}	0.0001	0.0008	m
tol_{ϵ_2}	0.0001	0.0008	m
D_{eye}	0.0001	1	m
δS_f^*	0	10	

Table 5.2: Performance Parameters with Suggested Values

Variable	Suggested Value	Units
$time_{move}$	5	s
$F_{humanmax}$	5	N
$max_{deadraysratio}$	0.35	
F_{human}	10	N
$MaxCost_{material}$	1,000	$\$$
$MaxCost_{tolerance}$	250,000	$\$$
$\frac{F}{n\sigma_{max}}$	5	
$\frac{F}{n\sigma_{min}}$	2.5	
τ_{max}	15	$N - m$
$tol_{perform}$	120	$\%$
$Vert_{L_{legs}}$	1.3	m
$time_{human}$	0.5	s
w	0.25	rad

Table 5.3: Hard Parameters with Values

Variable	Suggested Value	Units
$\alpha_{thermal_{tube}}$	$2.353 \cdot 10^{-5}$	$\frac{1}{\vartheta C}$
$\alpha_{thermal_{mirror}}$	$3.25 \cdot 10^{-6}$	$\frac{1}{\vartheta C}$
ΔT	20	C
d_{plo}	0.0254	m
$numrays$	200	
E_{legs}	$9.5 \cdot 10^{10}$	Pa
g	9.81	$\frac{m}{s^2}$
ρ_{tube}	2823	$\frac{kg}{m^3}$
t_{mirror}	0.00635	m
ρ_{mirror}	2230	$\frac{kg}{m^3}$
ρ_{legs}	1700	$\frac{kg}{m^3}$
ρ_{sch}	2519	$\frac{kg}{m^3}$
CR_{tube}	5437	$\frac{s}{m^3}$
CR_{sch_A}	3.4727	
CR_{sch_B}	23.415	
CR_{mirror_A}	366.1	
CR_{mirror_B}	-20.1	
CR_{legs}	368900	$\frac{s}{m^3}$
t_{tube}	0.005	m
d_{plo}	0.005	m
CRA_{slot}	1	
CRB_{slot}	0.005	
CRA_{stamp}	10	
CRB_{stamp}	0.05	
\hat{m}_2	-4	

Bibliography

- [1] Ces selector version 4.6.1, 2006, 1, 31, 1.
- [2] K.W. Chase, B.G. Loosi, W.H. Greenwood, and Hauglund L.F. Least cost tolerance allocation for mechanical assemblies with automated process selection. *Manufacturing Review*, 3:49–59, March 1990.
- [3] Murnaghan Instruments Corp. "astronomy" telescopes, dobsonian kits, telescope mirrors, parts, Accessed: December 12, 2006.
- [4] Esco Products Inc. Aspheric lenses, optical crown glass, Accessed December 12, 2006.
- [5] Harrie Rutten and Martin van Verooij. *Telescope Optics: Evaluation and Design*. Willmann-Bell, Inc., 1988.
- [6] Warren J. Smith. *Practical Optical System Layout*. McGraw-Hill, Inc., 1997.
- [7] V. Yu. Terebizh. Optimal baffle design in a cassegrain telescope. *Experimental Astronomy*, 11:171–191, 2001.
- [8] R.N. Wilson. *Reflecting Telescope Optics I*. Springer-Verlag Berlin Heidelberg, Inc., 1996.